INTERNATIONAL JOURNAL FOR NUMERICAL METHODS IN FLUIDS
Int. J. Numer. Meth. Fluids 2010; **63**:249–268
Published online 19 March 2009 in Wiley InterScience (www.interscience.wiley.com). DOI: 10.1002/fld.2025

Numerical methods for low-order modeling of fluid flows based on POD

J. Weller[1,2], E. Lombardi[2,3], M. Bergmann[1,2] and A. Iollo[1,2,*,†]

[1]*INRIA Bordeaux Sud Ouest, Team MC2, 351, Cours de la Libération, 33405 Talence cedex, France*
[2]*Institut de Mathématiques de Bordeaux, Université Bordeaux 1, UMR 5251 CNRS, 351, Cours de la Libération, 33405 Talence cedex, France*
[3]*Dipartimento Ingegneria Aerospaziale, Università di Pisa, Via G. Caruso 8, 56122 Pisa, Italy*

SUMMARY

This paper explores some numerical alternatives that can be exploited to derive efficient low-order models of the Navier–Stokes equations. It is shown that an optimal solution sampling can be derived using appropriate norms of the Navier–Stokes residuals. Then the classical Galerkin approach is derived in the context of a residual minimization method that is similar to variational multiscale modeling. Finally, calibration techniques are reviewed and applied to the computation of unsteady aerodynamic forces. Examples pertaining to both non-actuated and actuated flows are shown. Copyright © 2009 John Wiley & Sons, Ltd.

Received 4 December 2008; Revised 29 January 2009; Accepted 30 January 2009

KEY WORDS: proper orthogonal decomposition; reduced-order model

1. INTRODUCTION

Low-order modeling based on proper orthogonal decomposition (POD [1]) is an art based on physical intuition and numerical analysis. Very few results exist in terms of error bounds [2] as compared with other methods such as balanced truncation [3] for which precise estimates of the deviation of the reduced model from the full model exist. In turn, POD models can be applied to non-linear problems and it is computationally feasible for flows involving a large number of degrees of freedom. Low-order modeling is based on a number of assumptions affected by a certain degree of arbitrariness. The first choice is relative to the low-dimensional subspace where the solution is sought. In POD, this is done by extracting from an existing database the most energetic structures

*Correspondence to: A. Iollo, INRIA Bordeaux Sud Ouest, Team MC2, 351, Cours de la Libération, 33405 Talence cedex, France.
†E-mail: angelo.Iollo@math.u-bordeaux1.fr

in an average sense. Of course, in terms of L^2 approximation of the space spanned by the database, such a basis is optimal. However, the energy norm is not the only legitimate choice: for example, enstrophy provides an optimal representation of the database vorticity and in many detached flows one may assume that the rotational large-scale structures are the most dynamically relevant. Or, in order to provide the correct rates of dissipation, the H^1 norm can be used to take into account the relevance of smaller scales [4]. Besides the norm, the sampling of the flow field represents an implicit choice of the representation subspace, since the POD modes are just linear combinations of solution snapshots: the events collected in the snapshot database determine the approximation properties of the resulting POD modes. In this sense, the placement of the snapshots can be chosen so that the resulting modes minimize the projection error for a given number of snapshots and dimension of the reduced subspace, as a problem parameter is perturbed [5]. Another option, that we detail in the following, is to sample the flow so that the residuals of the high-fidelity operator are minimized over a range of parameter values. All these ideas aim at retrieving modes leading to accurate and robust dynamical systems describing the time evolution of the system.

The reduced-order dynamical system can be obtained in a number of different ways. The most popular procedure is that of representing by a modal expansion the velocity field and hence projecting the Navier–Stokes equations (NSE) over the velocity modes. The projection step is usually performed in the L^2 sense (see for example, [1, 6]), although in principal one could choose a different scalar product [7]. In some flow configurations the resulting pressure term is either zero or negligible, and therefore there is no need to model pressure. There are cases where this is not true [8], typically for internal flows. In addition pressure is needed both for computing forces and to evaluate the high-fidelity model residuals. It may be therefore necessary to model or estimate pressure effects. Another way of obtaining a low-order model is to minimize the high-fidelity model residuals in some norm. By minimizing high-fidelity residuals it is very simple to include integral constraints in the low-order model [9]. In general, this method leads to low-order models that have a different dynamical behavior as compared with models obtained by Galerkin projection.

The simple choice of how to discretize the derivatives of the POD modes has a dramatic impact on the asymptotic solution because of pure numerical effects. Truncation of the model also plays a crucial role in that the non-resolved modes strongly affect the dissipation rate of the model as well as the energy redistribution between scales. Numerical as well as modelization issues strongly affect the performance of the model in a manner that it is not easily predictable for complex flows. One way to circumvent this problem is to resort to model identification. The idea is to calibrate some of the coefficients appearing in the model against the reference simulation used to build the POD modes [10]. In other words, the modes as well as the model solution minimize the error both in terms of database representation and in time evolution. The advantage of this procedure is that it can be extended to several different databases so as to obtain a model that interpolates several dynamical behaviors [11]. In a different spirit, instead of identifying the model parameters, the effect on the resolved modes of the truncation can be modeled by appropriate closure terms. The procedure consists in assuming that the non-resolved scales are well represented by the residuals of the high-fidelity discrete operator [9], as it is done in some large-eddy simulation closure models [12]. In this sense, a modeling approach was recently proposed [13] in which the mode interactions are fed back in the dynamical system based on statistical information. The advantage of closure models is that they need far less coefficients to be tuned compared with calibration models.

In this paper, we show several examples of how the techniques used to model the NSE based on empirical eigenfunctions affect the accuracy and reliability of the results.

DOI: 10.1002/fld

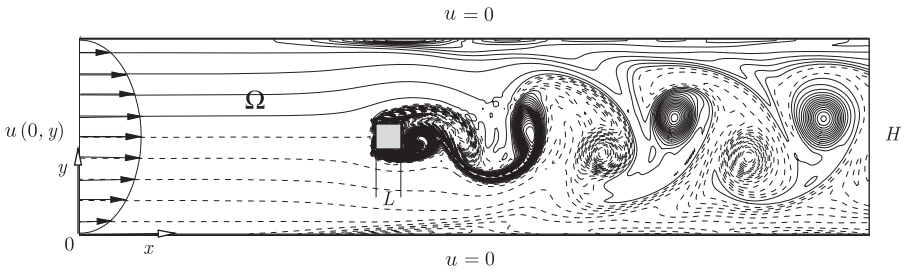

Figure 1. Flow configuration and vorticity snapshot at $Re=200$.

1.1. Numerical setup

Our test case is a two-dimensional incompressible laminar flow past a confined square cylinder (see Figure 1). The incoming flow has a Poiseuille profile. No-slip conditions are imposed on the cylinder and on the parallel walls. The blockage factor with reference with the figure is $L/H=\frac{1}{8}$. Details about numerical setup and method are reported in [14]. This is an interesting flow configuration as it involves detachment, wakes and interaction with walls. Another interesting point for reduced-order modeling purposes is that there is a pressure jump to model along the channel. Both controlled (see details in Section 5) and uncontrolled (Section 3 and Section 4) flows are considered.

2. MODELIZATION BY EMPIRICAL EIGENFUNCTIONS

The point of departure is a finite-dimensional representation: the solution is sought in a functional subspace V of dimension N_r that is built according to some desired properties

$$\bar{\mathbf{U}}(\mathbf{x},t)=\sum_{n=1}^{N_r} a_n(t)\boldsymbol{\Phi}_n(\mathbf{x}) \tag{1}$$

In the case of classical POD models, the functions $\boldsymbol{\Phi}_n(\mathbf{x})\in V$ give an optimal representation of precomputed solutions and there exist efficient ways to determine such functions [15]. We are however faced with a number of choices. First of all, one has to agree on a criteria for choosing N_r, i.e. the dimension of the projection space. This is usually done by fixing a threshold for the truncation error with respect to the precomputed database. In particular, we will show that the stability of a low-order model derived by a simple projection of the NSE strongly depends on the number of POD modes retained.

In addition, it has to be decided what we want to represent with $\bar{\mathbf{U}}(\mathbf{x},t)$, i.e. whether the velocity field and the pressure field are represented or not by two separate expansions. The expansion $\bar{\mathbf{U}}(\mathbf{x},t)$ may represent a $D=\{2,3\}$ dimensional vector field for the flow velocity, or a $D+1$ dimensional field also taking into account the pressure. In the first case, we need an additional finite-dimensional representation for pressure

$$\bar{p}(\mathbf{x},t)=\sum_{n=1}^{N_p} b_n(t)\psi_n(\mathbf{x}) \tag{2}$$

whereas in the latter case the pressure field is represented by one component of $\boldsymbol{\Phi}_n(\mathbf{x})$.

DOI: 10.1002/fld

However, coupling pressure and velocity fields has a certain degree of arbitrariness since at least for incompressible flows the actual value of pressure is unimportant. Pressure differences are important and hence in the definition of the norms leading to the velocity–pressure POD modes one implicitly makes a choice of the relative weight of velocity versus pressure.

We focus on the case where the velocity field and the pressure field are represented using two separate expansions, for the case where the POD modes include pressure, the following discussion is similar. The scalar coefficients $a_n(t), b_n(t)$ are unknowns and they can be found by using the governing equations. Let us define the residuals of the Navier–Stokes operator by

$$\mathscr{R}_M(\bar{\mathbf{U}}, \bar{p}) = \dot{a}_n \mathbf{\Phi}_n + a_n a_m (\mathbf{\Phi}_n \cdot \nabla)\mathbf{\Phi}_m + b_k \nabla \psi_k - a_n \Delta \mathbf{\Phi}_n \tag{3}$$

$$\mathscr{R}_C(\bar{\mathbf{U}}) = a_n \nabla \cdot \mathbf{\Phi}_n \tag{4}$$

where summation is taken over repeated indexes and $m, n = 1, \ldots, N_r, k = 1, \ldots, N_p$. In the case of usual POD modes, the residuals relative to continuity equations are identically zero as the velocity modes are the linear combinations of velocity flow snapshots. However, in more general cases, see, for example, [9], this may not be the case. The usual approach to obtain a system of ordinary differential equations (ODEs) from the residuals is that of using a Galerkin approach that consists in imposing that the residuals are orthogonal to the space spanned by the POD modes. Let the L^2 scalar product over (Ω) be $\langle \cdot, \cdot \rangle_\Omega$, and the induced energy norm $\| \cdot \|_\Omega$, we have

$$\langle \mathscr{R}_M(\bar{\mathbf{U}}, \bar{p}), \mathbf{\Phi}_n \rangle_\Omega = 0, \quad n = 1, \ldots, N_r \tag{5}$$

where Ω is the flow domain. When the velocity modes are not divergence free we have also

$$\langle \mathscr{R}_C(\bar{\mathbf{U}}), \psi_n \rangle_\Omega = 0, \quad n = 1, \ldots, N_p \tag{6}$$

If the POD velocity modes are divergence free, integration by parts of the pressure term in Equation (5) eliminates pressure from the equations, except for a boundary term. This term is usually neglected although it plays a crucial role in internal flows, where it represents the forcing term due to pressure drop. Of course, when the POD modes are divergence free, Equation (6) is identically satisfied. Otherwise, it represents a constraint in the integration of Equation (5). The Galerkin approach is well suited for linear elliptic partial differential equations (PDEs) for which, under certain assumptions, there exist proofs of well posedness as well as precise error bounds. In fluid flows, the problem is non-linear and dominated by advection; therefore, we cannot make use of such results and it is difficult, hence, to justify this choice on solid ground. Moreover, it can be shown that advection-dominated flows give rise to POD Galerkin models that are numerically unstable [4].

Another class of methods results from the idea of minimizing the norm of the residuals. Let us consider the general case of velocity modes that are not divergence free, and let the scalar product over space (Ω) and time ($[0, T]$) be $\langle \cdot, \cdot \rangle_\Omega^T$, and the induced energy norm $\| \cdot \|_\Omega^T$. The unknown functions $a_i(t)$ and $b_n(t)$ are represented by a spectral formulation over appropriate collocation points, i.e.

$$a_i(t) = \sum_{r=1}^{N_t} \hat{a}_{ir}\, \varphi_r(t), \quad b_n(t) = \sum_{r=1}^{N_t} \hat{b}_{nr}\, \varphi_r(t)$$

DOI: 10.1002/fld

where $\hat{a}_{ir}$ and $\hat{b}_{nr}$ are the values of the function at the collocation points and $\varphi_r(t)$ are Lagrange interpolating polynomials. We are left with $(N_r+N_p)\times N_t$ unknowns that solve

$$\min_{\hat{a}_{nr},b_n}(\|\mathscr{R}_M(\bar{\mathbf{U}},\bar{p})\|_\Omega^{\mathrm{T}}+\tau_C\|\mathscr{R}_C(\bar{\mathbf{U}})\|_\Omega^{\mathrm{T}}) \tag{7}$$

where $\tau_C\in\mathbb{R}^+$ is a penalization weight for the continuity equation. The necessary conditions for the minimum result in the following non-linear system of algebraic equations:

$$\forall l\in\{1,\ldots,N_t\},\quad \forall i\in\{1,\ldots,N_r\}\quad\text{and}\quad \forall n\in\{1,\ldots,N_p\}$$

$$\langle\dot{\varphi}_l\mathbf{\Phi}_i+\varphi_l\mathscr{L}_i(\bar{\mathbf{U}}),\mathscr{R}_M(\bar{\mathbf{U}},\bar{p})\rangle_\Omega^{\mathrm{T}}+\tau_C\langle\varphi_l\nabla\cdot\mathbf{\Phi}_i,\mathscr{R}_C(\bar{\mathbf{U}})\rangle_\Omega^{\mathrm{T}}=0 \tag{8}$$

$$\langle\varphi_l\nabla\psi_n,\mathscr{R}_M(\bar{\mathbf{U}},\bar{p})\rangle_\Omega^{\mathrm{T}}=0 \tag{9}$$

where

$$\mathscr{L}_i(\bar{\mathbf{U}})=(\bar{\mathbf{U}}\cdot\nabla)\mathbf{\Phi}_i+(\mathbf{\Phi}_i\cdot\nabla)\bar{\mathbf{U}}-\Delta\mathbf{\Phi}_i$$

In this formulation it is easy to include additional constraints. For example, it is possible to explicitly take into account the boundary conditions, or to satisfy known first integrals of the flow such as mass conservation. This can be done by including additional penalization terms in the minimization of Equation (7).

Yet another option is that of relaxing the spectral ansatz for $a_i(t)$ and $b_n(t)$ and obtaining a set of ODEs from

$$\min_{a_n,b_n}(\|\mathscr{R}_M(\bar{\mathbf{U}},\bar{p})\|_\Omega+\tau_C\|\mathscr{R}_C(\bar{\mathbf{U}})\|_\Omega) \tag{10}$$

which results in

$$\langle\mathscr{L}_i(\bar{\mathbf{U}}),\mathscr{R}_M(\bar{\mathbf{U}},\bar{p})\rangle_\Omega+\tau_C\langle\nabla\cdot\mathbf{\Phi}_i,\mathscr{R}_C(\bar{\mathbf{U}})\rangle_\Omega=0 \tag{11}$$

$$\langle\nabla\psi_n,\mathscr{R}_M(\bar{\mathbf{U}},\bar{p})\rangle_\Omega=0 \tag{12}$$

that can be written as $\forall i\in\{1,\ldots,N_r\},\forall n\in\{1,\ldots,N_p\}$. This is a set of non-linear algebraic-differential equations for $a_i(t)$ and $b_n(t)$. As mentioned, it may be practical to include pressure together with the velocity vector in the correlation function to compute the POD modes. In this case, we have $a_n(t)=b_n(t)$ and the above system reduces to the following system of ODEs $\forall i\in\{1,\ldots,N_r\}$:

$$\langle\mathscr{L}_i(\bar{\mathbf{U}})+\nabla\psi_i,\mathscr{R}_M(\bar{\mathbf{U}},\bar{p})\rangle_\Omega+\tau_C\langle\nabla\cdot\mathbf{\Phi}_i,\mathscr{R}_C(\bar{\mathbf{U}})\rangle_\Omega=0 \tag{13}$$

In Section 4, we will see that this approach is closely linked to recent stabilization methods used in finite elements.

We could minimize the residuals with respect to $\dot{a}_n$, but this would lead to the classical Galerkin method. What is used in practice is a blend of the two approaches

$$\langle\mathbf{\Phi}_i+\tau_M(\mathscr{L}_i(\bar{\mathbf{U}})+\nabla\psi_i),\mathscr{R}_M(\bar{\mathbf{U}},\bar{p})\rangle_\Omega+\tau_C\langle\nabla\cdot\mathbf{\Phi}_i,\mathscr{R}_C(\bar{\mathbf{U}})\rangle_\Omega=0 \tag{14}$$

with $\tau_M\in\mathbb{R}^+$ and $\forall i\in\{1,\ldots,N_r\}$.

DOI: 10.1002/fld

The models proposed above enjoy different numerical properties. For example, it is known that the Galerkin approach is unstable and that the least-square approach is dissipative. However, a common problem is that these models are not robust with respect to variations of physical parameters such as the Reynolds number or the effect of a control. Therefore, it was proposed to introduce a calibration of the model [16] that would modify all or a part of the constant coefficients resulting from the different projection methods presented above, in order to match as close as possible the time evolution of the reference simulations. This will be explained in more details in Section 5.

3. SAMPLING OF THE INPUT SYSTEM PARAMETERS SUBSPACE

The main drawback of POD basis functions is that they are only able to give an optimal representation of the kinetic energy included in the snapshot database. Usually, this database is collected from a flow generated with some given system input parameters. Thus, the same basis functions are not optimal for representing characteristics of another flow generated with different system input parameters (see [17–19]). The aim of this section is therefore to give an efficient criterion to sample the input parameter subspace in order to improve the robustness of the POD basis functions. For simplicity reasons, the input parameter subspace is reduced to a Reynolds number interval $\mathscr{I}=[Re_L, Re_R]$, where we chose $Re_L=70$ and $Re_R=180$. These values correspond approximately to the lower and higher bound for the 2D periodic regime for the confined square cylinder wake flow. Numerically, $\mathscr{I}$ is disrcetized with $\Delta Re=5$, and is denoted $\mathscr{I}_h$. We note that all the concepts introduced in this study can be easily extended to higher-dimensional control spaces, as done in Reference [5].

The number of snapshots N_s to be collected in order to perform a POD analysis is flow dependent. The objective is to capture all the temporal frequencies by a sufficient sampling. An *a posteriori* check on the adequacy of the database can be performed by verifying if the retained POD modes do not vary when additional snapshots are included in the database. By proceeding in this way the sampling is sufficient although is not necessarily optimal.

In order to improve the functional subspace, we want to enlarge the database in an iterative way by adding some snapshot sets that correspond to different Reynolds numbers $Re_i \in \mathscr{I}$. Let $U^{[Re_1,\ldots,Re_N]}$ be the database composed by N snapshots sets taken independently at $Re_1,\ldots,Re_N$, where the parameter N has to be determined according to the desired accuracy of the POD basis. The main question is to determine how to chose these Reynolds numbers to compute a robust POD basis $\mathbf{\Phi}(\mathbf{x})$ from database $U^{[Re_1,\ldots,Re_N]}$ so that the POD flow field reconstruction $\bar{\mathbf{U}}(\mathbf{x}, t)$ (see Equation (1)) is as close as possible to the numerical solution of the NSE, $\mathbf{U}(\mathbf{x}, t)$, for all Reynolds numbers in $\mathscr{I}_h$. Note that we will always use $N_r=50$ basis functions, even if $N>1$ Reynolds numbers are considered. The temporal coefficients $a_n(t)$ are evaluated by projecting the numerical solution of the NSE onto the POD basis functions, i.e.

$$a_n(t)=\int_\Omega \mathbf{U}(\mathbf{x}, t)\mathbf{\Phi}_n(\mathbf{x})\,\mathrm{d}\mathbf{x} \tag{15}$$

Two class of sampling methods are commonly used for POD. The first one is based on the Centroidal Voronoi Tessellations (CVT, see [20–22]) that can be efficiently computed using the Lloyd algorithm [23]. The drawback of such an approach is that the number of sampling points has to be fixed meaning that we cannot control the degree of accuracy. The second one is based

DOI: 10.1002/fld

on Greedy sampling (see [5]). This is an iterative sampling for which we can choose the degree of accuracy by fixing a stopping criterion. In this study we will present a hybrid sampling method that couples both ideas.

To illustrate our sampling method, we will consider an initial database $U^{[Re_1]}$ composed of N_s snapshots collected at $Re_1 = 100$. Note that we will always use $N_s = 200$ in this study, so the database $U^{[Re_1,\ldots,Re_k]}$ is composed of $k \times N_s$ snapshots. As we can see in Figure 2, the error defined by

$$\langle \mathbf{U}' \rangle_2 = \int_T \|\mathbf{U}'(\mathbf{x}, t)\|_2 \, \mathrm{d}t \tag{16}$$

where $\mathbf{U}'(\mathbf{x}, t) = \mathbf{U}(\mathbf{x}, t) - \bar{\mathbf{U}}(\mathbf{x}, t)$ denotes the missing scales, grows when we move away from the sampling point $Re_1 = 100$. Indeed, we have $\langle \mathbf{U}' \rangle_2 \propto |Re - Re_1|$. The Greedy method consists in sampling the input parameter subspace where the error is maximal, namely

$$Re_k^{\mathrm{GRE}} = \arg \max_{Re} \langle \mathbf{U}' \rangle_2 \tag{17}$$

For instance $Re_2^{\mathrm{GRE}} = 180$ in Figure 2. In order to reduce the CPU costs, one usually uses the residual of the Navier–Stokes operator evaluated with the POD flow field reconstruction, $\bar{\mathbf{U}}$ (see Equation (1)), denoted $\mathscr{R}_M(\bar{\mathbf{U}})$, instead of using the error (16) (see [5]). Using such an approximation, the new points $Re_k, k = 2, \ldots, N$ can be computed as being the centroids of the Greedy region (CGR) $\mathscr{I}_k^{GRE}$

$$Re_k^{CGR} = \frac{\int_{\mathscr{I}_k^{\mathrm{GRE}}} Re\,\rho(Re)\,\mathrm{d}Re}{\int_{\mathscr{I}_k^{\mathrm{GRE}}} \rho(Re)\,\mathrm{d}Re} \quad \text{with } \rho(Re) = \langle \mathscr{R}_M(\bar{\mathbf{U}}) \rangle_2 \tag{18}$$

where the Greedy region is

1. centred on the Greedy value Re_K^{GRE},
2. with radius $\min_{i \in [1; N-1]} |Re_K^{\mathrm{GRE}} - Re_i|$,
3. restricted to $\mathscr{I}_K^{\mathrm{GRE}} \subset \mathscr{I}$.

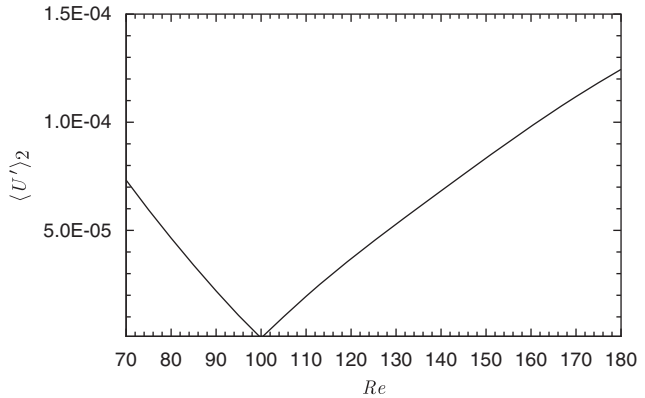

Figure 2. Evolution of the error $\langle \mathbf{U}' \rangle_2$ versus the Reynolds number.

DOI: 10.1002/fld

Table I. Evolution of the average error (19) versus the number of CGR sampling points.

k	1	2	3	4	5
Re_k^{CGR}	100	152	81	170	126
$\mathscr{J}_k^{\mathrm{CGR}}$	60×10^{-4}	16×10^{-4}	7.7×10^{-4}	3.6×10^{-4}	3.0×10^{-4}
Re_k^{GRE}	100	180	70	140	80
$\mathscr{J}_k^{\mathrm{GRE}}$	$60\times19\cdot2^{-4}$	19.2×10^{-4}	12.9×10^{-4}	6.1×10^{-4}	4.5×10^{-4}

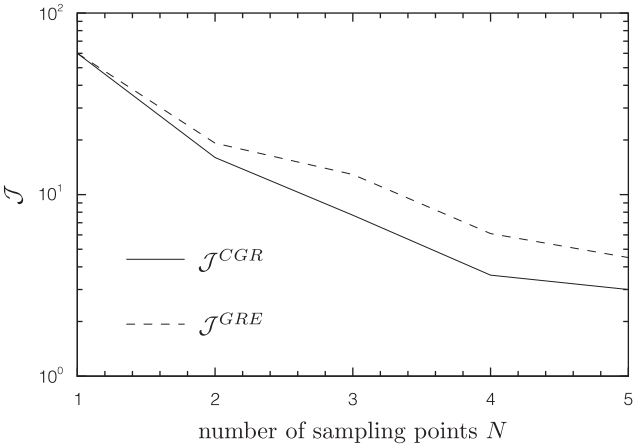

Figure 3. Evolution of the average error $\mathscr{J}$ versus the number of sampling points for the centroidal Greedy region (CGR) and the Greedy (GRE) sampling methods.

Note that this criterion can be easily transposed for input parameter subspaces with dimension greater than one. For instance, the Greedy regions are intervals, disks, spheres and hyper-spheres for dimensions 1, 2, 3 and greater than 3, respectively.

We can see in Table I that this criterion enables a significant reduction of the average error, noted $\mathscr{J}$, evaluated on the input parameter subspace $\mathscr{I}$ under consideration, i.e.

$$\mathscr{J}=\int_{\mathscr{I}}\langle\mathbf{U}'\rangle_2^2\,\mathrm{d}Re \tag{19}$$

This *a priori* centroidal Greedy region sampling method gives points that are more efficient than the Greedy ones (see Figure 3). Moreover, they are very close to the *a posteriori* optimal ones (see [24]).

4. MODEL BY CLOSURE TERMS

This section is devoted to stabilizing the reduced-order models by means of closure terms in the spirit of least-squares methods presented in Section 2. To be more precise the idea is to use the variational multiscale method (VMS, see [9, 12]) in order to take into account in the

DOI: 10.1002/fld

ROM the fine scales that are not calculated by standard POD-Galerkin ROMs. The VMS method is an improvement of the standard streamline upwind Petrov–Galerkin (SUPG). It is based on approximating the fine scales using the residuals of the Navier–Stokes operator computed with the truncated POD flow fields. In order to compute the Navier–Stokes residuals the pressure field is needed. We then use the pressure extended model introduced in Reference [9]

$$\sum_{j=1}^{N_r} L_{ij} \frac{\mathrm{d}a_j}{\mathrm{d}t} = \sum_{j=1}^{N_r} B_{ij} a_j + \sum_{j=1}^{N_r} \sum_{k=1}^{N_r} C_{ijk} a_j a_k \tag{20a}$$

with initial conditions

$$a_i(0) = (\mathbf{U}(\mathbf{x}, 0), \mathbf{\Phi}_i(\mathbf{x}))_\Omega, \quad i = 1, \ldots, N_r \tag{20b}$$

where $\mathbf{\Phi} = (\boldsymbol{\phi}, \psi)^{\mathrm{T}}$ denotes the POD basis. For the purpose of reduced-order modeling one wants to use a very small number N_r of POD basis functions in expansion (1). As it was already mentioned, the dissipative missing scales (high-order POD modes, namely $\mathbf{\Phi}_i$, $i > N_r$) are then not taken into account in the ROM. Thus, due to a lack of dissipation, the solution of ROM (20) can either converge toward erroneous limit cycles or even diverge in an exponential way (see Figure 4). It seems thus it is necessary to introduce into the ROM (20) the effects of the missing scales. In the spirit of the VMS method the missing scales $\mathbf{u}'$ and p' can be approximated using the residuals of the governing equations

$$\mathbf{u}' \simeq -\tau_M \mathscr{R}_M \tag{21a}$$

$$p' \simeq -\tau_C \mathscr{R}_C \tag{21b}$$

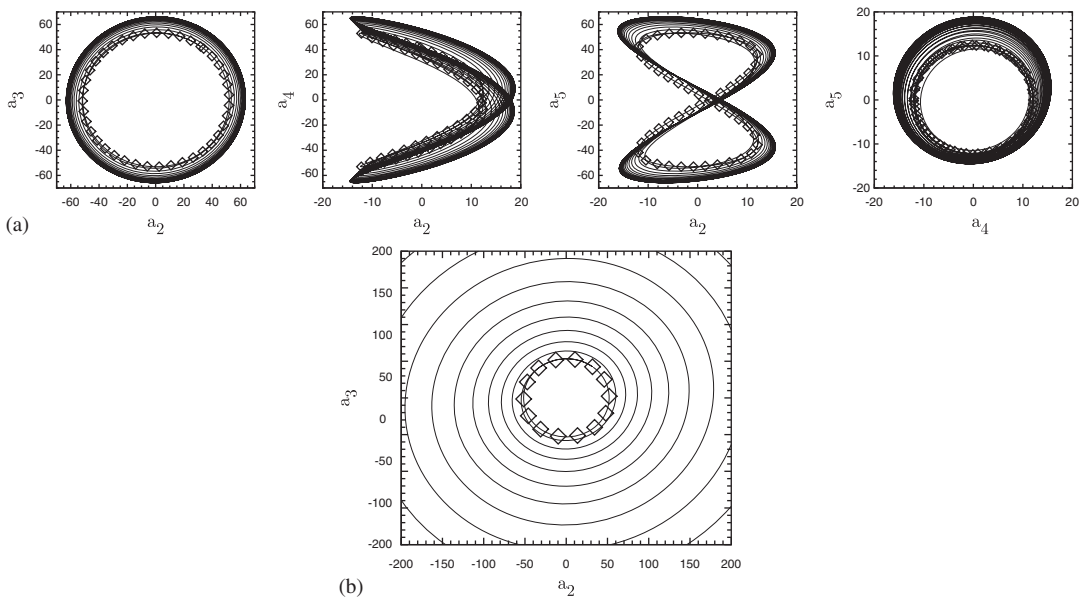

Figure 4. Comparison of the projected (NS: ◇) with the predicted (standard pressure ROM: —) limit cycles over 1000 vortex shedding periods.

DOI: 10.1002/fld

where τ_M and τ_C denote some constant parameters to be fixed. We recall that the vector functions $\mathscr{R}_M$ and $\mathscr{R}_C$ denote, respectively, the residuals of the momentum and continuity equations evaluated with the POD fields (1) with $\bar{\mathbf{U}}=(\bar{\mathbf{u}},\ \bar{p})^{\mathrm{T}}$. After some algebra manipulations, the VMS model is

$$\sum_{j=1}^{N_r} L_{ij}\frac{\mathrm{d}a_j}{\mathrm{d}t}=\sum_{j=1}^{N_r} B_{ij}a_j+\sum_{j=1}^{N_r}\sum_{k=1}^{N_r} C_{ijk}a_j a_k+F_i(t) \tag{22a}$$

with initial conditions

$$a_i(0)=(\mathbf{U}(\mathbf{x},0),\mathbf{\Phi}_i(\mathbf{x}))_\Omega,\quad i=1,\ldots,N_r \tag{22b}$$

where

$$\begin{aligned}F_i(t)=&(\bar{\mathbf{u}}\cdot\nabla\boldsymbol{\phi}_i+\nabla\psi_i,\ \tau_M\mathscr{R}_M(\mathbf{x},t))_\Omega+(\nabla\cdot\boldsymbol{\phi}_i,\ \tau_C\mathscr{R}_C(\mathbf{x},t))_\Omega\\&+(\bar{\mathbf{u}}\cdot(\nabla\boldsymbol{\phi}_i)^{\mathrm{T}},\tau_M\mathscr{R}_M(\mathbf{x},t))_\Omega\\&-(\nabla\boldsymbol{\phi}_i,\tau_M\mathscr{R}_M(\mathbf{x},t)\otimes\tau_M\mathscr{R}_M(\mathbf{x},t))_\Omega\end{aligned} \tag{23}$$

Note that neglecting the two last terms of (23) leads to the SUPG model. These two additional terms come from the variational multiscale developments described in Reference [12]. The VMS ROM (22) with (23) is then stable as one can see from the long time integration performed in Figure 5.

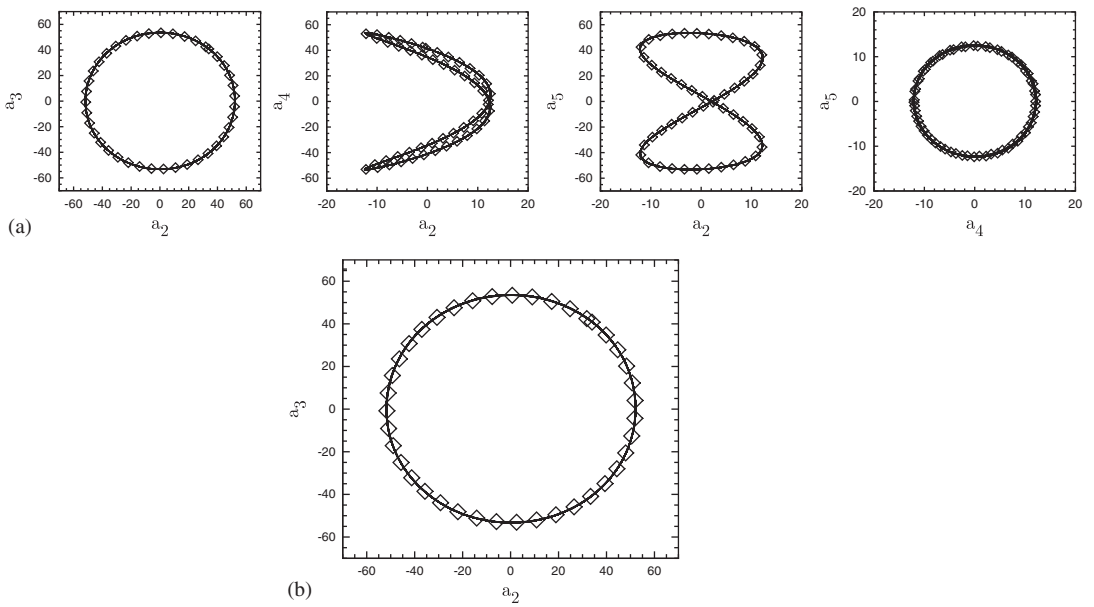

Figure 5. Comparison of the projected (NS: ◇) with the predicted (VMS ROM: —) limit cycles over 1000 vortex shedding periods.

DOI: 10.1002/fld

In comparison with the calibrated models introduced in Section 5.4, the VMS model requires the calibration[‡] of only two parameters, namely τ_M and τ_C. Moreover, the VMS model can be used for a very long time integration. Unfortunately, it is less obvious to fit the VMS model to several dynamics as it can be done using calibrated models.

5. MODEL BY CALIBRATION

5.1. Controlled flow setup

The controlled flow configuration is the same as that described in Section 1.1. The actuators are two jets placed on the upper and lower faces of the cylinder. The presence of the actuators is modeled by imposing a new boundary condition on a small surface Γ_c of the cylinder boundary:

$$\mathbf{u}(\mathbf{x},t)\cdot\mathbf{n}(\mathbf{x})=c(t),\quad \mathbf{x}\in\Gamma_c$$

The jets are normal to the walls and are driven in opposite phase, as shown in Figure 6:

$$v(\mathbf{x},t)=c(t),\quad \mathbf{x}\in\Gamma_c$$

For control purposes, using measurements of the vertical velocity at points $\mathbf{x}_j$ in the cylinder wake, we can define a proportional control law

$$c(t)=\sum_{j=1}^{N_v}\mathsf{K}_j v(\mathbf{x}_j,t)$$

where N_v denotes the number of sensors used. We could then use the model to compute the set of feedback gains K_j that minimizes the vortex shedding in the cylinder wake.

5.2. The POD basis

In our case, a numerical simulation of the NSE is performed over a time interval $[0,T]$, and the velocity field is saved at N_s time instants $t_i\in[0,T]$. This yields a data set $\{\mathbf{u}^i(\mathbf{x})=\mathbf{u}(\mathbf{x},t^i)\}_{i=1..N_s}$.

In the case of forced flow, the snapshots depend on the control law $c(t)$ used. In this section, we consider a classical POD basis derived from numerical simulations obtained using several different control laws $c(t)$ while all the other parameters (such as Reynolds number or domain geometry) will be the same.

The data set used for the POD is therefore written as

$$\{\mathbf{u}^{i,\ell}(\mathbf{x})=\}_{i=1..N_s,\ell=1..N_c}$$

where N_c denotes the number of control laws considered. If $\mathscr{C}=\{c_1,c_2,\ldots,c_{N_c}\}$ is the set of control laws used to obtain the database, the ensuing POD basis is denoted by $\boldsymbol{\phi}(\mathscr{C})$.

[‡]Note that these parameters can be found using some scaling arguments (see [25] for more details), so that no mobilization is required.

DOI: 10.1002/fld

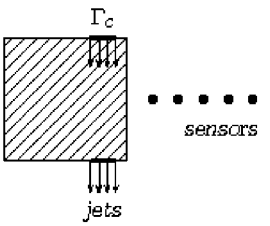

Figure 6. Placement of synthetic jet and sensors for control.

5.3. Dealing with the boundary conditions

In the non-controlled case, we lift the boundary conditions on the velocity fields by defining a new set of snapshots

$$\mathbf{w}^i(\mathbf{x}) = \mathbf{u}^i(\mathbf{x}) - \hat{\mathbf{u}}(\mathbf{x})$$

where $\hat{\mathbf{u}}$ is some reference velocity field that satisfies the same boundary conditions as the snapshots. In the present configuration, it can be the steady unstable solution or a time average of the snapshots $\mathbf{u}^k$.

When an extra boundary condition is imposed on the cylinder for control purposes, the snapshots are chosen to be

$$\mathbf{w}^i(\mathbf{x}) = \mathbf{u}^i(\mathbf{x}) - \hat{\mathbf{u}}(\mathbf{x}) - c(t^i)\mathbf{u}_c(\mathbf{x})$$

where $\mathbf{u}_c(\mathbf{x})$ satisfies the following criteria:

$$\mathbf{u}_c(\mathbf{x}) = \mathbf{0} \quad \text{on} \quad \Gamma \backslash \Gamma_c \quad \text{and} \quad \mathbf{u}_c(\mathbf{x}) = \mathbf{1} \quad \text{on} \ \Gamma_c$$

In practice we use the velocity field proposed in [16]

$$\mathbf{u}_c(\mathbf{x}) = \frac{1}{c^\star}(\hat{\mathbf{u}}'(\mathbf{x}) - \hat{\mathbf{u}}(\mathbf{x}))$$

where $\hat{\mathbf{u}}'$ is obtained in the same way as $\hat{\mathbf{u}}$ but applying a constant control equal to $c^\star$ on Γ_c . The low-dimensional solution is now written:

$$\bar{\mathbf{u}}(\mathbf{x}, t) = \hat{\mathbf{u}}(\mathbf{x}) + c(t)\mathbf{u}_c(\mathbf{x}) + \sum_{k=1}^{N_r} a_k(t)\boldsymbol{\phi}_j(\mathbf{x}) \tag{24}$$

5.4. POD-Galerkin reduced-order model with calibration

We consider the simple velocity model (as opposed to the pressure extended model (20)). Extra terms appear in the reduced-order model due to the presence of control:

$$\dot{a}_i(t) = A_i + B_{ij}a_j(t) + C_{ijk}a_j(t)a_k(t) + E_i\dot{c}(t) + F_i c^2(t) + G_i c(t) + H_{ij}a_j(t)c(t) \tag{25a}$$

with initial conditions

$$a_i(0) = \langle \mathbf{u}(\cdot, 0), \boldsymbol{\Phi}_i(\cdot) \rangle, \quad i = 1, \ldots, N_r \tag{25b}$$

DOI: 10.1002/fld

where

$$E_i = \langle \mathbf{u}_c, \boldsymbol{\phi}_i \rangle$$

$$G_i = -\langle (\hat{\mathbf{u}} \cdot \nabla)\mathbf{u}_c, \boldsymbol{\phi}_i \rangle - \langle (\mathbf{u}_c \cdot \nabla)\hat{\mathbf{u}}, \boldsymbol{\phi}_i \rangle + \frac{1}{Re}\langle \Delta \mathbf{u}_c, \boldsymbol{\phi}_i \rangle$$

$$F_i = \langle (\mathbf{u}_c \cdot \nabla)\mathbf{u}_c, \boldsymbol{\phi}_i \rangle$$

$$H_{ij} = \langle (\mathbf{u}_c \cdot \nabla)\boldsymbol{\phi}_j, \boldsymbol{\phi}_i \rangle + \langle (\boldsymbol{\phi}_j \cdot \nabla)\mathbf{u}_c, \boldsymbol{\phi}_i \rangle$$

Setting:

$$\mathbf{X}_i = [A_i, \{B_{ij}\}_{j=1,\ldots,N_r}, \{C_{ijk}\}_{j,k=1,\ldots,N_r}, E_i, F_i, G_i, \{H_{ij}\}_{j=1,\ldots,N_r}]^{\mathrm{T}}$$

and

$$\mathbf{f}(\mathbf{a}(t), c(t), \dot{c}(t)) = [1, \{a_j(t)\}_{j=1,\ldots,N_r}, \{a_j(t)a_k(t)\}_{j,k=1,\ldots,N_r}, \dot{c}(t), c^2(t), c(t), \{a_j(t)c(t)\}_{j=1,\ldots,N_r}]$$

the Equation (25a) can be written in the compact form:

$$\dot{a}_i(t) = \mathbf{f}(\mathbf{a}(t), c(t), \dot{c}(t)) \cdot \mathbf{X}_i$$

As discussed in several papers [16, 18, 26], the initial value problem (25) can be inaccurate, even unstable, for it may not take into account enough of the flow dynamics. Indeed, although a number N_r of modes can be sufficient to capture most of the flow energy, the neglected modes continue to play an important role in the flow dynamics through their interaction with the resolved ones.

In order to build a robust order model we applied the calibration technique described in [11]. Following that approach, the system coefficients contained in matrix $\mathbf{X}$ are adjusted to fit the solution of (25) to several dynamics.

We consider a database that includes simulations obtained with N_c different control laws to calculate the POD basis. The system coefficients obtained by Galerkin projection of the NSE on the N_c-*control* low-dimensional subspace are denoted $\widehat{\mathbf{X}}$. The calibration procedure then consists in choosing $\mathbf{X}$ as the solution of

$$\min_X \sum_{i=1}^{N_r} \sum_{\ell=1}^{N_c} \int_0^T (\dot{\hat{a}}_i^{\ell}(t) - \mathbf{f}(\hat{\mathbf{a}}^{\ell}(t), c^{\ell}(t), \dot{c}^{\ell}(t)) \cdot \mathbf{X}_i)^2 \mathrm{d}t + \alpha \sum_{r=1}^{N_r} \|\mathbf{X}_i - \widehat{\mathbf{X}}_i\|^2 \tag{26}$$

where

$$\hat{a}_i^{\ell}(t) = \langle \mathbf{u}^{\ell}(\cdot, t), \boldsymbol{\phi}_i \rangle$$

and where α is the Tikhonov regularization parameter and is chosen $\ll 1$. Following the idea of [10], all the elements of $\mathbf{X}$ are calibrated except the N_r^3 terms C_{ijk}. We recall that this is due to the assumption that the errors in the Galerkin model are mainly due to the fact that it neglects the small scales and therefore a large part of the viscous effects, and C_{ijk} results from the projection of the convective term.

We refer to a model built using N_c control laws as an N_c-control model. Such a model is denoted by $\mathscr{M}(\mathscr{C})$ where $\mathscr{C} = \{c_1, \ldots, c_{N_c}\}$.

DOI: 10.1002/fld

5.5. Lift and drag modeling

In this section we present a technique for evaluating the forces on the body using the POD model developed. We define the lift and the drag coefficients on the square cylinder in the classical way

$$C_L(t) = \frac{\int_S ((p(\mathbf{x},t)-p_0)\cdot\bar{\mathbf{n}}(\mathbf{x}) + \tau(\mathbf{x},t)\cdot\bar{\mathbf{t}}(\mathbf{x}))\,\mathrm{d}S}{\frac{1}{2}U_0^2 S}\cdot\bar{\mathbf{j}}$$

$$C_D(t) = \frac{\int_S ((p(\mathbf{x},t)-p_0)\cdot\bar{\mathbf{n}}(\mathbf{x}) + \tau(\mathbf{x},t)\cdot\bar{\mathbf{t}}(\mathbf{x}))\,\mathrm{d}S}{\frac{1}{2}U_0^2 S}\cdot\bar{\mathbf{i}}$$

where p_0, U_0 are the reference pressure and velocity at the inflow and τ is the viscous stress tensor.

In order to calculate the lift and drag coefficients we have to provide an estimation of the pressure field around the square cylinder. A POD procedure is performed also for the pressure fields. This leads to a set of POD pressure modes ψ_n. The pressure at each time instant can be developed in terms of the first N_r^p modes

$$\bar{p}(\mathbf{x},t) = \hat{p}(\mathbf{x}) + c(t)\,p_c(\mathbf{x}) + \sum_{i=1}^{N_r^p} b_i(t)\psi_i(\mathbf{x}) \tag{27}$$

where $\hat{p}(\mathbf{x})$ and $p_c(\mathbf{x})$ are the pressure fields of the same reference solutions used to satisfy the boundary conditions for the velocity.

We recall the Poisson equation for incompressible flows:

$$\Delta p(\mathbf{x},t) = -\nabla\cdot(\mathbf{u}(\mathbf{x},t)\cdot\nabla\mathbf{u}(\mathbf{x},t)) \tag{28}$$

Using the expansion for $\bar{p}(\mathbf{x},t)$ and $\bar{\mathbf{u}}(\mathbf{x},t)$ in terms of the first N_r and N_r^p modes, respectively, and given a control law $c(t)$, the projection of the Poisson equation onto the retained pressure modes leads to the following system:

$$\begin{aligned} L_{il}^p b_l(t) &= A_i^p + B_{ij}^p a_j(t) + C_{ijk}^p a_j(t)a_k(t) + F_i^p c^2(t) + G_i^p c(t) + H_{ij}^p a_j(t)c(t) \\ &1 \leqslant i, \quad l \leqslant N_r^p \\ &1 \leqslant j, \quad k \leqslant N_r \end{aligned} \tag{29}$$

where

$$L_{ij}^p = (\Delta\psi_j, \psi_i)$$

$$A_i^p = -(\Delta\hat{p}, \psi_i) - (\nabla\cdot(\hat{\mathbf{u}}\cdot\nabla\hat{\mathbf{u}}, \psi_i))$$

$$B_{ij}^p = -((\nabla\cdot(\hat{\mathbf{u}}\cdot\nabla\boldsymbol{\phi}_j), \psi_i) - (\nabla\cdot(\boldsymbol{\phi}_j\cdot\nabla\hat{\mathbf{u}}), \psi_i))$$

$$C_{ijk}^p = -(\nabla\cdot(\boldsymbol{\phi}_j\cdot\nabla\boldsymbol{\phi}_k), \psi_i)$$

$$G_i^p = -((\nabla\cdot(\hat{\mathbf{u}}\cdot\nabla\mathbf{u}_c)), \psi_i) - ((\nabla\cdot(\mathbf{u}_c\cdot\nabla\hat{\mathbf{u}})), \psi_i) - (\Delta p_c, \psi_i)$$

$$F_i^p = -((\nabla\cdot(\mathbf{u}_c\cdot\nabla\mathbf{u}_c)), \psi_i)$$

$$H_{ij}^p = -((\nabla\cdot(\mathbf{u}_c\cdot\nabla\boldsymbol{\phi}_j)), \psi_i) - ((\nabla\cdot(\boldsymbol{\phi}_j\cdot\nabla\mathbf{u}_c)), \psi_i)$$

DOI: 10.1002/fld

We denote this model $\mathscr{P}(\mathscr{C})$ where $\mathscr{C}=\{c_1,\ldots,c_{N_c}\}$ is again the set of control laws used to obtain the database. This model enables to calculate the pressure coefficients $b_i(t)$ at each time instant at which the velocity coefficients $a_i(t)$ are known.

In order to fit the pressure model to the database solutions, we again perform a multiple control calibration procedure described above (26) for the Poisson model. We let $\hat{b}_i(t)$ be the temporal coefficients obtained by projecting the pressure (calculated by solving the NSE) onto the POD subspace. The coefficients $\mathbf{X}^p$ are chosen by minimizing the norm of the residual obtained by substituting $\hat{b}_i(t)$ into (29) (as previously C^p_{ijk} results from the Galerkin projection and is not calibrated).

Once the dynamic low-order model $\mathscr{M}(\mathscr{C})$ is integrated the calculated velocity coefficients $a_r(t)$ are used with the model $\mathscr{P}(\mathscr{C})$ in order to estimate the pressure coefficients $b_r(t)$. Both sets of coefficients are then used to estimate the lift and drag coefficients.

5.6. Results

The described technique was applied in order to build a low-order model of the actuated flow around a confined square cylinder for Reynolds number $Re=150$, with feedback control laws. Different velocity models with one and more control laws and their predictions with different controls are analyzed in [11]. As in [11] actuation by jets is started only once the flow is fully developed. With the control turned on the simulation is performed for about seven shedding cycles, and $N_s\approx 200$ snapshots are saved. The non-dimensional duration of the time interval is $T\simeq 50$. The number of POD modes retained for the reduced-order model for the velocity is $N_r=60$.

We chose three different feedback configurations that give three control laws, which we denote $c_1(t)$, $c_2(t)$ and $c_3(t)$, shown in Figure 7. The figure also shows the drag coefficients obtained for each control law. For each control law a simulation of the NSE is performed and 200 snapshots are saved for each simulation. We then defined two control sets, a 1-control set and a 2-control set

$$\mathscr{C}^2=\{c_2\}$$

$$\mathscr{C}^{1,2}=\{c_1,c_2\}$$

For each $\mathscr{C}^i$, we computed a POD basis $\boldsymbol{\phi}(\mathscr{C}^k)$ as described in Section 5.2 and a calibrated reduced-order model $\mathscr{M}^k=\mathscr{M}(\mathscr{C}^k)$ by solving problem (26). The control law $c_3(t)$ was chosen to be a *test control law*, and was used as input for the NSE and for the reduced-order models $\mathscr{M}(\mathscr{C}^k)$ defined above.

The first aim of calibration, which is attained with the above method, is that a model $\mathscr{M}(\{c\})$ fitted to a certain control, provides accurate results when integrated with that control. However, for estimation and control purposes the model needs to be accurate when integrated with different control laws. The benefit of using N_c-control models with $N_c>1$ was shown in [11]. To illustrate this point we consider the projection of the solution induced by c_3 onto the POD subspaces $\text{span}\{\boldsymbol{\phi}(\mathscr{C}^k)\}$ (for $k=2$ and $k=(1,2)$), and the solutions obtained by solving systems $\mathscr{M}^k$ with input c_3. Model $\mathscr{M}^2$ could be expected to give better results than model $\mathscr{M}^{1,2}$ due to the fact that the dynamics induced by c_3 are *closer* to those induced by c_2 than to those induced by c_1. This can be seen by comparing the coefficients resulting from the projections onto $\text{span}\{\boldsymbol{\phi}(\mathscr{C}^{1,2})\}$ of the three different solutions, or by comparing the resulting lift coefficients (see Figure 7). However, model $\mathscr{M}^{1,2}$ turns out to give a lower reconstruction error than $\mathscr{M}^2$. Estimations of the third modal coefficient by the 1- and the 2-control models are plotted in Figure 8.

DOI: 10.1002/fld

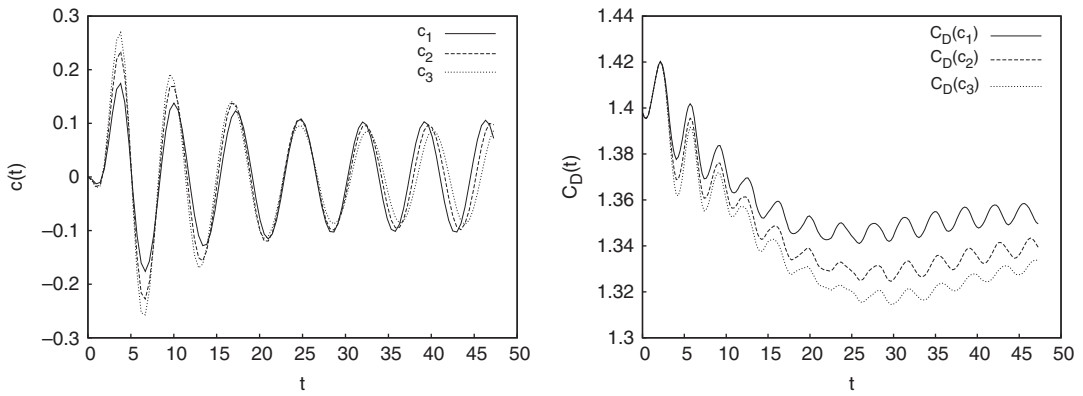

Figure 7. Control laws used for building and testing the model and corresponding lift coefficients.

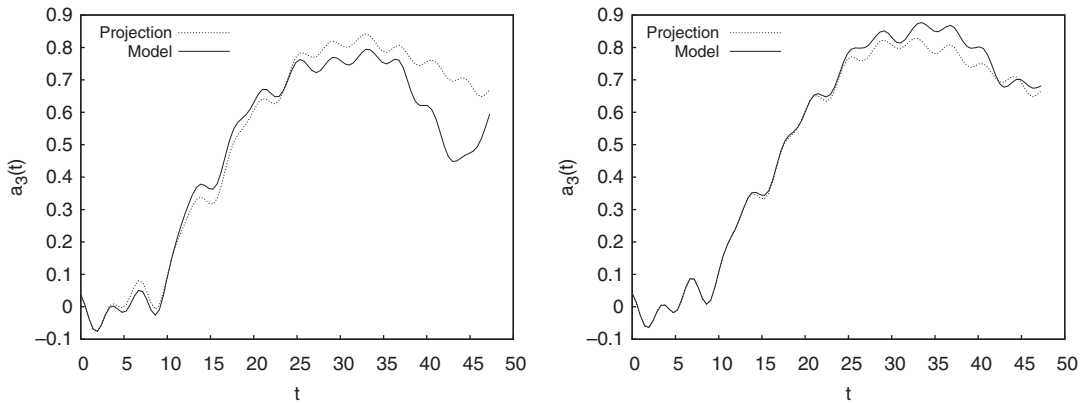

Figure 8. $\hat{a}_3$ DNS versus a_3 obtained by model integration $\mathscr{M}^2$ (left) and $\mathscr{M}^{1,2}$ (right) using c_3.

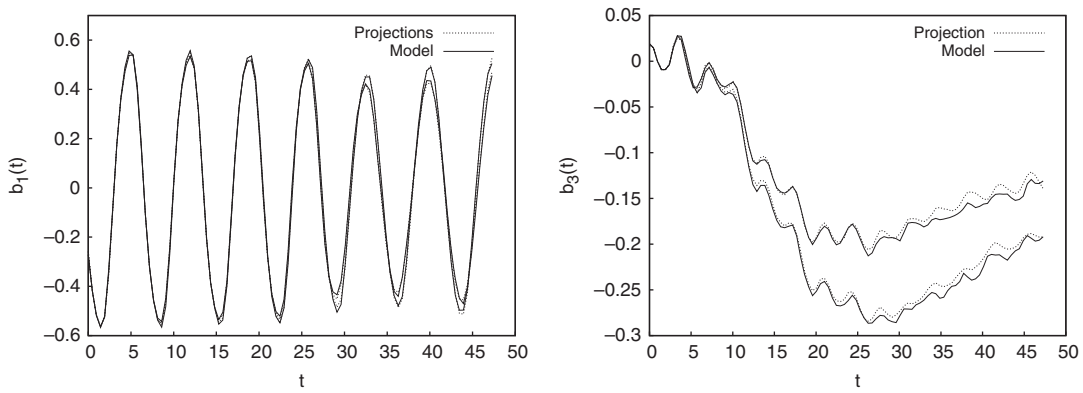

Figure 9. $\hat{b}_1$ and $\hat{b}_3$ DNS versus b_1 and b_3 obtained by model integration $\{\mathscr{M}^{1,2} - \mathscr{P}^{1,2}\}$ using c_1 and c_2.

DOI: 10.1002/fld

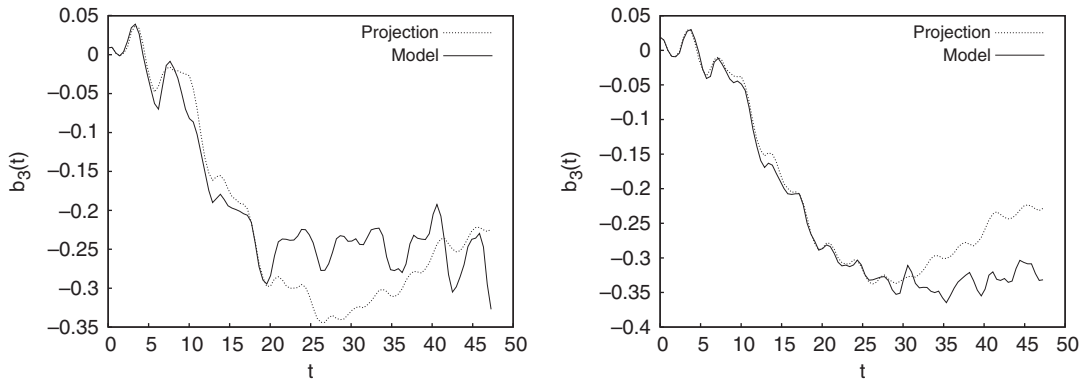

Figure 10. $\hat{b}_3$ DNS versus b_3 obtained by model integration $\{\mathscr{M}^2-\mathscr{P}^2\}$ (left) and $\{\mathscr{M}^{1,2}-\mathscr{P}^{1,2}\}$ (right) using c_3.

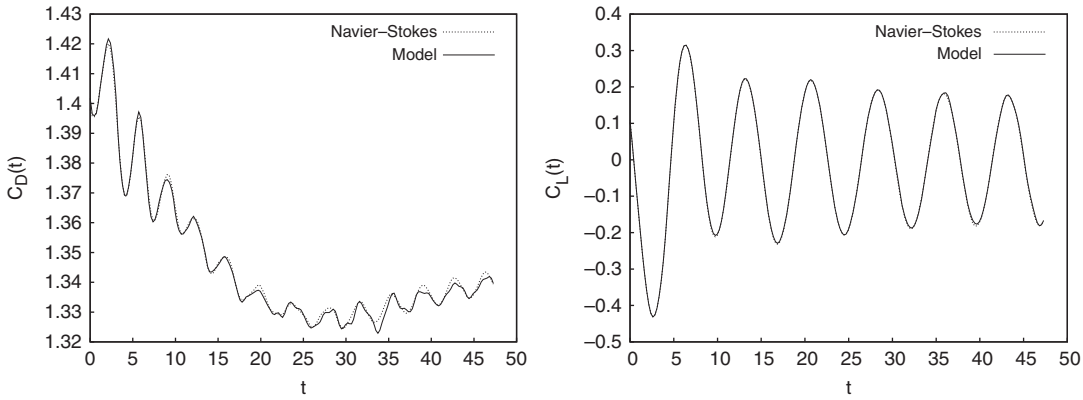

Figure 11. C_D and C_L DNS versus C_D and C_L obtained by model integration of $\{\mathscr{M}^2-\mathscr{P}^2\}$ using c_2.

The modal coefficients $a_i(t)$ given by the two models $\mathscr{M}^k$ are then used in the pressure models $\mathscr{P}^k$ to obtain the pressure modal coefficients $b_i(t)$. The number of POD pressure modes retained is $N_r^p=60$. Figure 9 shows the estimations of some coefficients resulting from solving $\{\mathscr{M}^{1,2}-\mathscr{P}^{1,2}\}$ with $c=c_1$ and $c=c_2$. In this example, the 2-control velocity–pressure model provides a good approximation of the pressure coefficients for the two dynamics that it was fitted to by calibration.

In Figure 10 the same coefficients are plotted when the dynamic models are integrated using the test control law c_3. The results obtained with the 1-control model are also shown: for approximation of the pressure coefficients the 2-control model gives better results than the 1-control model.

We now look at the velocity–pressure model's capacity to predict the time history of the drag and lift coefficients. Figure 11 shows the lift and drag coefficients resulting from integrating model $\{\mathscr{M}^2-\mathscr{P}^2\}$ with $c=c_2$. The 1-control model proves to be able to reproduce the forces on the cylinder for the dynamic to which it was fitted. Figure 12 shows similar results obtained with the 2-control model.

DOI: 10.1002/fld

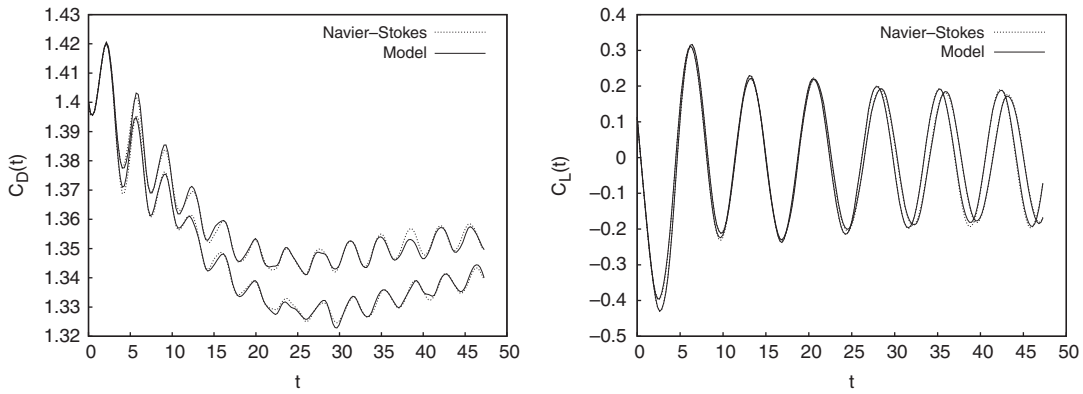

Figure 12. C_D and C_L DNS versus C_D and C_L obtained by model integration of $\{\mathscr{M}^{1,2}-\mathscr{P}^{1,2}\}$ using c_1 and c_2.

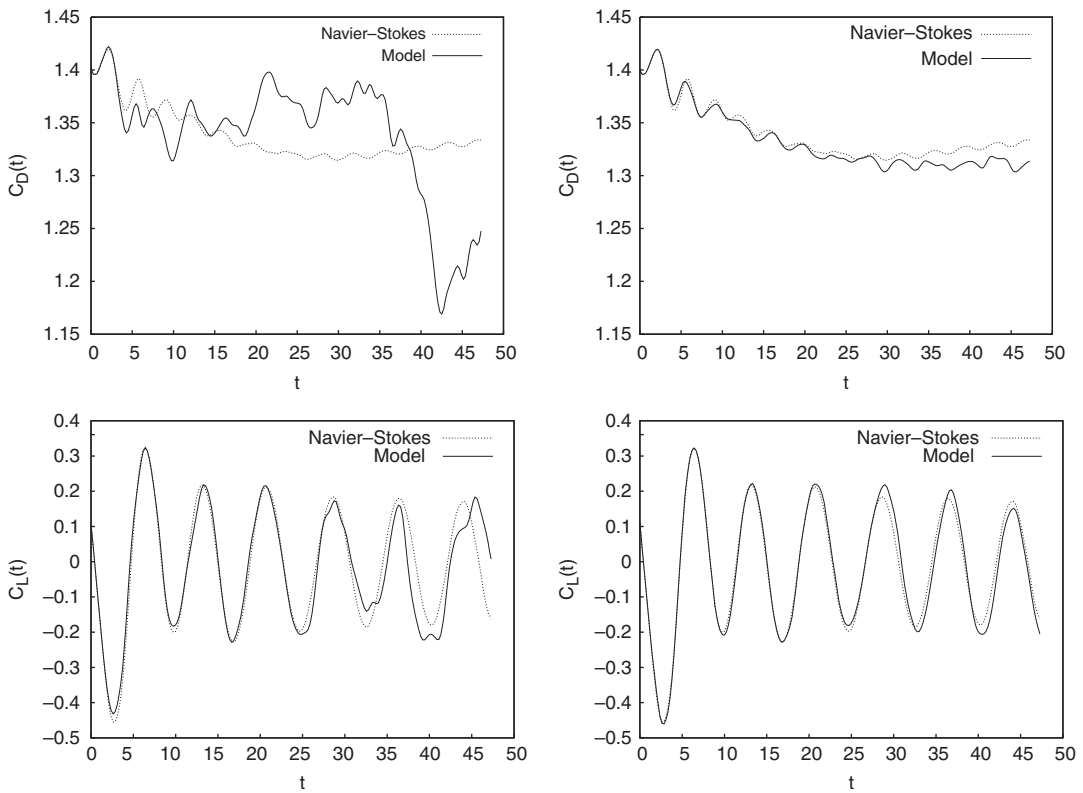

Figure 13. C_D and C_L DNS versus C_D and C_L obtained by models integration $\{\mathscr{M}^{2}-\mathscr{P}^{2}\}$ (left) and $\{\mathscr{M}^{1,2}-\mathscr{P}^{1,2}\}$ (right) using c_3.

DOI: 10.1002/fld

In Figure 13 the DNS lift and drag coefficients are shown together with the predictions of the 1-control and 2-control models. The figure shows that the 2-control model is able to almost perfectly reconstruct the coefficients over a limited time interval, while the 1-control model diverges after only a few time steps.

6. CONCLUSIONS

In this paper we emphasize the different numerical choices that lead to a low-order model. We do not provide a detailed analysis of each option; however, we present numerical evidences to illustrate the discussion. We considered a low-order model that includes pressure and that is obtained in a Galerkin-least-squares framework. It is based on a closure term that can be interpreted either as the modelization of the effect of the small scales on the large ones, or as a classical penalization term. This model is stable for configurations where classical POD models are unstable. Future work will be devoted to extend the Galerkin-least-squares model to control configurations. On the other hand, we showed how robust models can be obtained by identifying a set of parameters appearing in the system of ODEs. This procedure enables, for example, the prediction of aerodynamic forces with a good degree of accuracy. Finally, we showed that the optimal solution sampling leads to significantly lower representation errors in terms of the POD modes. To make this option viable, we plan to use the reduced-order model to make the sampling process more efficient.

REFERENCES

1. Lumley JL. The structure of inhomogeneous turbulent flows. In *Atmospheric Turbulence and Radio Wave Propagation*, Yaglom AM, Tatarski VL (eds). Nauka: Moscow, 1967; 166–178.
2. Hinze M, Volkwein S. Proper orthogonal decomposition surrogate models for nonlinear dynamical systems: error estimates and suboptimal control. *Dimension Reduction of Large-scale Systems* 2005; 261–306.
3. Antoulas AC. *Approximation of Large-Scale Dynamical Systems*. SIAM: Philadelphia, PA, 2005.
4. Iollo A, Lanteri S, Desieri JA. Stability properties of pod-Galerkin approximations for the compressible Navier–Stokes equations. *Theoretical and Computational Fluid Dynamics* 2000; **13**:377–396.
5. Bui-Thanh T, Willcox K, Ghattas O. Model reduction for large-scale systems with high-dimensional parametric input space. *SIAM Journal on Scientific Computing* 2008; **30**(6):3270–3288.
6. Aubry N, Holmes P, Lumley JL, Stone E. The dynamics of coherent structures in the wall region of a turbulent boundary layer. *Journal of Fluid Mechanics* 1988; **192**:115–173.
7. Iollo A, Dervieux A, Desieri JA, Lanteri S. Two stable pod-based approximations to the Navier–Stokes equations. *Computing and Visualization in Science* 2000; **3**:61–66.
8. Noack B, Papas P, Monkewitz P. The need for a pressure-term representation in empirical galerkin models of incompressible shear flows. *Journal of Fluid Mechanics* 2005; **523**:339–365.
9. Bergmann M, Bruneau C, Iollo A. Enablers for robust pod models. *Journal of Computational Physics* 2009; **228**(2):516–538.
10. Galletti B, Bruneau CH, Zannetti L, Iollo A. Low-order modelling of laminar flow regimes past a confined square cylinder. *Journal of Fluid Mechanics* 2004; **503**:161–170.
11. Weller J, Lombardi E, Iollo A. Robust model identification of actuated vortex wakes. *Physica D*: *Nonlinear Phenomena* 2009; **238**(4):416–427.
12. Bazilevs Y, Calo VM, Cottrell JA, Hugues TJR, Reali A, Scovazzi G. Variational multiscale residual-based turbulence modeling for large eddy simulation of incompressible flows. *Computer Methods in Applied Mechanics and Engineering* 2007; **197**:173–201.
13. Noack BR, Schlegel M, Ahlborn B, Mutschke G, Morzynski M, Comte P, Tadmor G. A finite-time thermodynamics formalism for unsteady flows. *Journal of Non-equilibrium Thermodynamics* 2008; **3**(2):103–148.
14. Buffoni M, Camarri S, Iollo A, Salvetti M. Low-dimensional modelling of a confined three dimensional wake flow. *Journal of Fluid Mechanics* 2006; **569**:141–150.

DOI: 10.1002/fld

15. Sirovich L. Turbulence and the dynamics of coherent structures. Parts I, II and III. *Quarterly of Applied Mathematics* 1987; **XLV**:561–590.
16. Galletti B, Bottaro A, Bruneau C, Iollo A. Accurate model reduction of transient flows. *European Journal of Mechanics—B*: *Fluids* 2006; **26**:354–366.
17. Prabhu RD, Collis SS, Chang Y. The influence of control on proper orthogonal decomposition of wall-bounded turbulent flows. *Physics of Fluids* 2001; **13**(2):520–537.
18. Bergmann M, Cordier L, Brancher J-P. Optimal rotary control of the cylinder wake using proper orthogonal decomposition reduced-order model. *Physics of Fluids* 2005; **17**:097–101.
19. Bergmann M, Cordier L. Optimal control of the cylinder wake in the laminar regime by trust region methods and pod reduced-order models. *Journal of Computational Physics* 2008; **227**(16):7813–7840.
20. Du Q, Faber V, Gunzburger MD. Centroidal voronoi tessellations: applications and algorithms. *SIAM Review* 1999; **41**(4):637–676.
21. Burkardt J, Gunzburger MD, Lee HC. Centroidal voronoi tessellation-based reduced-order modeling of complex systems. *Technical Report*, Florida State University, 2004.
22. Burkardt J, Gunzburger MD, Lee HC. Centroidal voronoi tessellation-based reduced-order modeling of complex systems. *SIAM Journal on Scientific Computing* 2007; **28**(2):459–484.
23. Du Q, Emelianenko M, Ju L. Convergence of the Lloyd algorithm for computing centroidal voronoi tessellations. *SIAM Journal on Numerical Analysis* 2007; **44**(1):102–119.
24. Bergmann M, Iollo A. Improving proper orthogonal decomposition robustness by optimal sampling. *Research Report*, INRIA 2009.
25. Hugues TJR, Feijoo G, Mazzei L, Quincy JB. The variational multiscale method—a paradigm for computational mechanics. *Computer Methods in Applied Mechanics and Engineering* 1998; **166**:3–24.
26. Couplet M, Basdevant C, Sagaut P. Calibrated reduced-order pod-Galerkin system for fluid flow modelling. *Journal of Computational Physics* 2005; **207**(1):192–220. DOI: http://dx.doi.org/10.1016/j.jcp.2005.01.008.